

# Autofocusing and trapping performance of circular swallowtail beams on Rayleigh particles

Huanpeng Liang<sup>1</sup>, Kaijian Chen<sup>1</sup>, Nana Liu<sup>1</sup>, Liu Tan<sup>1</sup>, Fuxi Lu<sup>1</sup>, Shaozhou Jiang<sup>1</sup>, And Yi Liang<sup>1,\*</sup>

<sup>1</sup>Guangxi Key Lab for Relativistic Astrophysics, Center on Nanoenergy Research, School of Physical Science and Technology, Guangxi University, Nanning, Guangxi 530004, China

\* liangyi@gxu.edu.cn

**Abstract:** Circular swallowtail beams (CSBs) have garnered significant attention due to their remarkable autofocusing capabilities, making them highly promising for applications such as optical trapping. In this study, we conducted a comprehensive investigation into the autofocusing behavior and trapping forces of CSBs. Our findings reveal that CSBs exhibit optimal autofocusing performance when the radius of the main ring is approximately half of the CSB radius. Moreover, we observed that the focal length of CSBs consistently surpasses that of circular Airy beams, even under identical initial conditions. Through experimental observations, we confirmed the autofocusing propagation of CSBs. Furthermore, we theoretically analyzed the trapping force and stability of CSBs on Rayleigh particles. Our results unequivocally demonstrate that CSBs possess excellent trapping capabilities, indicating their immense potential in optical manipulation and trapping applications.

## 1. Introduction

Various accelerating beams that propagate along curved trajectories have attracted a lot of attentions due to a huge potential for many applications including optical tweezers[1-3], biomedical science[4], astrophysics[5]and so on. The most famous accelerating beams, named Airy beams[6-12], are experimentally generated in 2007. Airy beams can be described as a result of the fold catastrophe in catastrophe theory. There are seven fundamental catastrophes including fold, cusp, swallowtail, butterfly, elliptical umbilic, hyperbolic umbilic, and parabolic umbilic. Most beams related to these catastrophes can present a curve propagation trajectory, i.e., can be employed to generate an accelerating beam. For example, a family of accelerating beams, called Pearcey beams[13, 14], comes from the cusp catastrophe. Recently, originating from swallowtail catastrophe, a new kind of high-order accelerating beams named Swallowtail beams are generated [15]. Swallowtail beams exhibit a unique feature: by tuning control parameters, Swallowtail beams not only can evolve into higher-order butterfly catastrophes during propagation, but also can decay to lower-order cuspsoids such as Pearcey beams. As we know, the autofocusing property of autofocusing beams[16-20]generated from accelerating beams is determined by the acceleration of the beams. For instances, circular Airy beams (CABs) modulate their autofocusing propagation by tuning the parameters related to acceleration of Airy beams including the scale factor and initial position of main lobe[21]. Along this line, one can infer that autofocusing beams based on Swallowtail beams such as Circular swallowtail beams (CSBs) also show a similar autofocusing progress, as demonstrated in Refs.[22-29].

Due to such autofocusing property, CSBs show a much strong intensity contrast at autofocusing positions, implying a huge application potential on optical manipulation or trapping. However, as far as we know trapping force and the trapping stability of CSBs lack of systematic study. Especially, a comparison between CSBs and CABs with same conditions is still absent. Thus, in this work, we not only do further research on the autofocusing propagation property of CSBs in theory and experiment, but also explore the trapping capability of CSBs on Rayleigh particles in theory. We demonstrate the trapping ability of CSBs theoretically, and the trapping-force can be changed by tuning the scale factor and the radius of initial main ring. Our work provides a comprehensive understanding on the optical trapping capabilities of CSBs, promoting new tools for optical manipulation and trapping.

## 2. Theory

In the catastrophe theory, a standard diffraction integral is given by[23]:

$$C_n = \int_{-\infty}^{+\infty} \exp[ip_n(a, s)] ds \quad (1)$$

where  $p_n(a, s)$  is the canonical potential function that can determine the properties of the caustic field, and it is defined by[23]:

$$p_n(a, s) = s^n + \sum_{j=1}^{n-2} a_j s^j \quad (2)$$

Here,  $a_j$  is a control parameter and  $s^j$  is a state parameter. Usually, a Swallowtail beam can be expressed by the swallowtail catastrophe integral[25]:

$$Sw(X, Y, Z) = \int_{-\infty}^{+\infty} \exp\left(i\left(s^5 + Zs^3 + Ys^2 + Xs^1\right)\right) ds \quad (3)$$

where  $X = x/x_0, Y = y/y_0$  denote the dimensionless coordinates in the real space, and  $x_0, y_0$  are the scaling factors which can be arbitrary adopted.

For simply constructing a circular swallowtail beam, Eq. (3) is transformed into a new expression in cylindrical coordinates[25]:

$$\Phi(r, \theta, 0) = Sw\left(\frac{r_0 - r}{x_0}, 0, 0\right) \delta(r, \theta) \quad (4)$$

where  $r_0$  is the initial radius of the main ring and  $x_0$  is the scale factor, which determines the width of ring, and  $\delta(r, \theta)$  is the optical aperture to make the energy of beam finite for experimental realization, which is defined as follows:

$$\delta(r, \theta) = \begin{cases} 1, 0 \leq r \leq R_B, 0 \leq \theta \leq 2\pi \\ 0, other. \end{cases} \quad (5)$$

Where  $R_B$  is the radius of the CSBs in the initial plane.

In paraxial approximation, Swallowtail beam propagates following the below wave equation[25]:

$$2i \frac{\partial \Phi}{\partial \xi} + \frac{\partial^2 \Phi}{\partial r^2} + r^{-1} \frac{\partial \Phi}{\partial r} + r^{-2} \frac{\partial^2 \Phi}{\partial \theta^2} = 0 \quad (6)$$

Then, similar to the previous works[30, 31], we can apply beam propagation methods to simulate the propagation of CSBs and analyze their autofocusing property.

### 3. Simulation and Experiment of propagation of CSBs

As shown in the Fig. 1(d), in experiment, CSBs are generated by means of hologram[25, 27, 28]. The hologram is loaded in a transmissive spatial light modulator(SLM) (1024×768, pixel pitch is 36  $\mu m$ , fill factor is 58%). A linear polarized Gaussian beam is emitted from the semiconductor laser (532nm), and then are expanded by the lens (L1 and L2). After passing through the SLM, such beam is transferred into a CSB with sufficient information by a 4f system (L3 and L4). Finally, the initial intensity distribution of the CSB appears in the focal plane of L4 and the propagation of CSBs can be recorded by moving the CCD camera slowly.

In the simulation, the parameters are set as  $R_B = 1.4mm, r_0 = 0.7mm, x_0 = 8.33\mu m$ , the incident power is kept as 1W. Figures 1(a1-a3) display the numerical propagation results of CSBs including the intensity of propagation of CSBs at  $z=0mm, 61mm, 75mm$  ( $z$  is the longitudinal distance of propagation). Clearly, at the beginning, the main ring of CSB possesses the most power when CSB is generated in Fig. 1(a1). When the beam comes to the position of  $z=61mm$  [Fig. 1(a2)], all power automatically focuses at a very small spot whose radius is about 8  $\mu m$ , obviously exhibiting a autofocusing property without any lens in free space. After the focus, the power gradually spreads out of the focus [Fig. 1(a3)]. Figs. 1(b1-b3) shows the corresponding experimental results at  $z=0mm, 61mm, 75mm$ . One can find that the experimental results are basically consistent with the numerical results. Figures 1(c1-c2) are the side-views of numerical and experimental propagations, where the dash lines depict the trajectory of the main ring and autofocusing is observed clearly. Fig. 1(c3) is the sideview autofocusing profile where an intensity ratio is used to define

the intensity contrast:  $K = I_{max} / I_0$ ,  $I_{max}$  is the max intensity of focus and  $I_0$  is the max intensity of initial plane. As shown in Fig. 1(c3), the intensity of CSB abruptly increases near the focus and the focal length is 61mm.

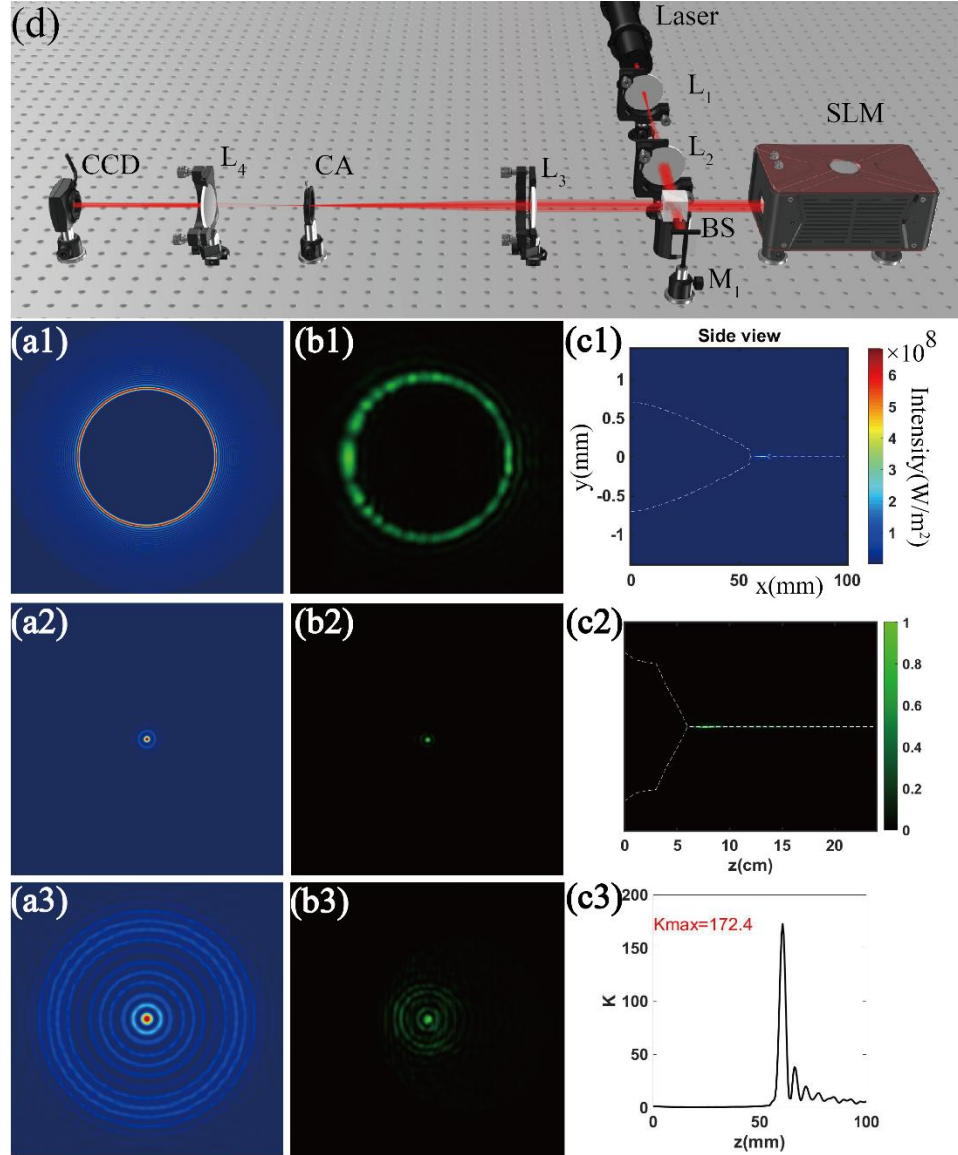


Fig. 1 Propagation of CSBs.  $R_b = 1.4\text{mm}, r_0 = 0.7\text{mm}, x_0 = 8.33\ \mu\text{m}$ . (a1-a3) are numerical results at  $z=0\text{mm}, 61\text{mm}, 75\text{mm}$ . (b1-b3) are experimental results at  $z=0\text{mm}, 61\text{mm}, 75\text{mm}$ . (c1) is the numerical side-view, (c2) is the experimental side-view. (c3) is the numerical autofocusing profile. (d) is experimental setup: Laser(532nm), semiconductor laser. M, mirror. L, lens. BS, beam splitter. SLM, spatial light modulator. CA, aperture.

#### 4. The tunable autofocusing property of CSBs

Next, we systematically analyze how the parameters of CSBs to control their autofocusing property and present a comparison with CABs at the same conditions. For simple discussion, we apply the same intensity ratio  $K$  in Fig. 1(c3) to represent the autofocusing ability and keep the incident power 1W.

In Fig. 2(a),  $R_b$  is set to be 1mm. Clearly,  $K$  increases as  $x_0$  becomes smaller, and the best autofocusing performance appears when  $r_0 \approx 0.5R_b$ . The intensity contrast  $K$  can reach 70. In Fig. 2(b), the  $R_b$  is changed to 1.4mm, and  $r_0$  corresponding to the best autofocusing performance is approximately 0.7mm,

i.e., still a half of  $R_B$ . Generally, CSBs show the best autofocusing performance as long as  $r_0$  is approximately a half of  $R_B$ . Fig. 2(c) illustrates the varying autofocusing performance of CABs when the control parameters are changed. Also, the  $K$  of CABs ( $\sim Ai\left(\frac{r_0-r}{x_0}\right) \exp\left(a\frac{r_0-r}{x_0}\right)$ ) increases while  $x_0$  becomes smaller, but CABs show the largest intensity contrast at  $r_0 \approx 0.3R_B$  when  $R_B$  is still set to be 1mm. Incidentally, for both of the CSBs and CABs, when  $x_0$  is too small,  $r_0$  cannot be set too small. Otherwise, the beams would not automatically focus at a point because the main ring determined by  $r_0$  is too small to form the autofocusing of these circular autofocusing beams. Furthermore, from Fig. 2(d), one can observe that, the focal length of CSBs is always longer than the focal length of CABs when  $x_0$  and  $r_0$  are set as the same. Whatever, both of CABs and CSBs present longer autofocusing lengths when  $x_0$  and  $r_0$  become larger to generate a wider initial main ring. A wider initial main ring implies a beam require a longer propagation distance to focus itself into a small spot due to the main contribution to autofocusing of main ring.

## 5. The trapping force of CSBs on Rayleigh particle

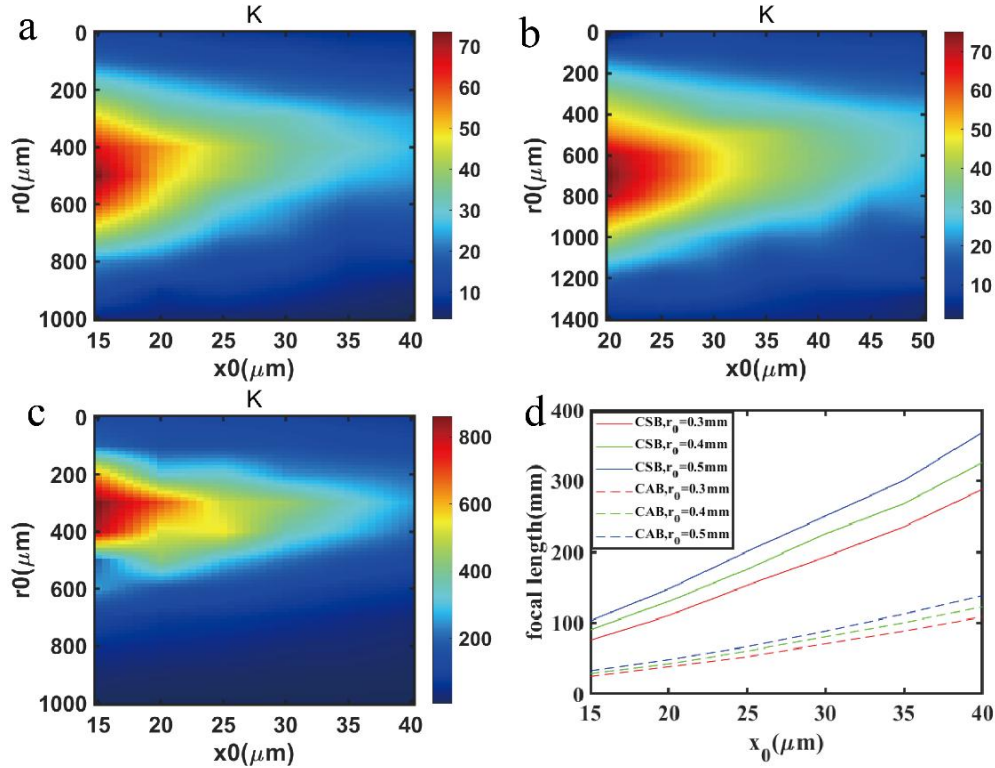


Fig. 2 the intensity contrast  $K$  of CSBs and CABs with different parameters. (a) CSB,  $R_B = 1mm$ . (b) CSB,  $R_B = 1.4mm$ . (c) CAB,  $R_B = 1mm, a = 0$ . (d) The variation of focal length of CSBs and CABs with scale factor and radius ( $R_B = 1mm$ ).

According to the theory, the gradient force  $\overline{F}_g$  and the scattering force  $\overline{F}_s$  of Rayleigh particle can be calculated by[21, 32]:

$$\overline{F}_g = \frac{1}{4} \varepsilon_0 \varepsilon_m \operatorname{Re}(\alpha) \nabla \left| \overline{\Phi}^2 \right| \quad (7)$$

$$\overline{F}_s = \frac{\varepsilon_0 \varepsilon_m^3 k_0^4}{12\pi} |\alpha^2| \left| \overline{\Phi}^2 \right| \quad (8)$$

where  $\varepsilon_m$  is the dielectric of the medium around the particle,  $\varepsilon_0$  is the dielectric of the constant in vacuum.  $k_0$  is the wave number in vacuum. The polarizability  $\alpha$  is[21]:

$$\alpha = 4\pi R_p^3 \frac{\varepsilon_p - \varepsilon_m}{\varepsilon_p + 2\varepsilon_m} \quad (9)$$

where  $R_p$  is the radius of Rayleigh particles.

Based on Eqs. (7) and (8), we obtain the distributions of the longitudinal and transverse radiation force of CSBs (the focal length is 2.835mm), as shown in Fig. 3. Here,  $\lambda = 1064\text{nm}$ ,  $R_b = 0.2\text{mm}$ ,  $r_0 = 50\mu\text{m}$ ,  $x_0 = 5\mu\text{m}$ , the radius of particle  $R_p$  is 20nm, the refractive index of the surrounding medium (water)  $n_m$  is 1.33, the refractive index of polystyrene particle  $n_p$  is 1.573, and  $\varepsilon_m = n_m^2$ ,  $\varepsilon_p = n_p^2$ .

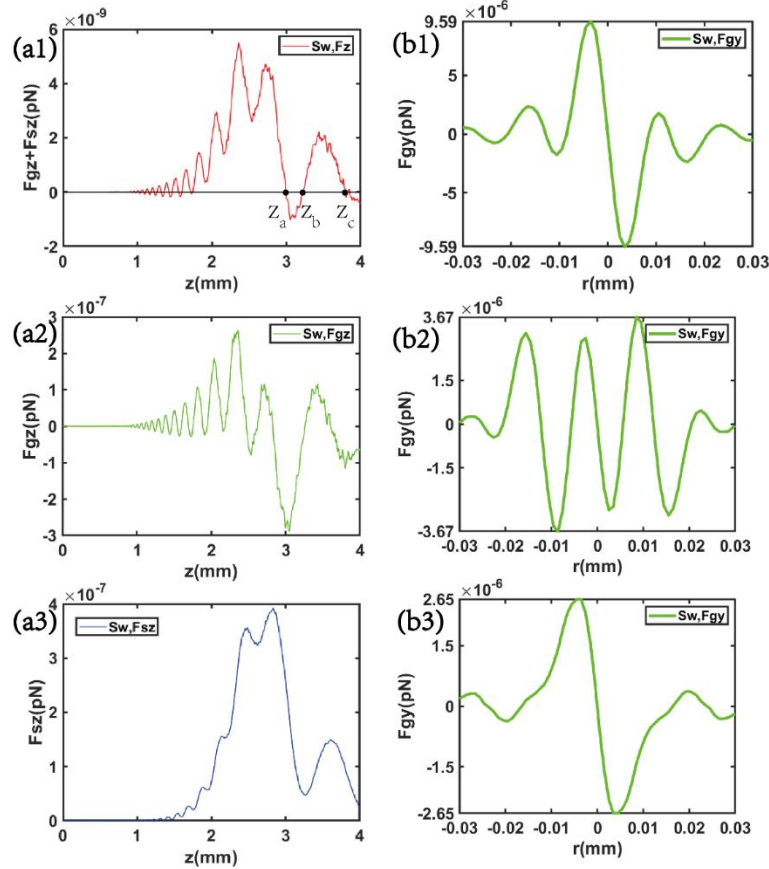


Fig. 3 The trapping force of CSBs on the 20nm polystyrene particle with  $\lambda = 1064\text{nm}$ ,  $R_b = 0.2\text{mm}$ ,  $r_0 = 50\mu\text{m}$ ,  $x_0 = 5\mu\text{m}$ , the incident power is 1 W and Focal length is 2.835mm. (a1) the sum of longitudinal gradient force and longitudinal scattering force with  $z_a=2.983\text{mm}$ ,  $z_b=2.991\text{mm}$ ,  $z_c=2.999\text{mm}$ . (a2) the longitudinal gradient force. (a3) the longitudinal scattering force. (b1-b3) the corresponding transverse gradient force at the three points  $z_a$ ,  $z_b$ ,  $z_c$ .

From Fig. 3 (a), one can infer that, the particle will be trapped at  $z_a=2.983\text{mm}$ ,  $z_b=2.991\text{mm}$ ,  $z_c=2.999\text{mm}$  in the propagation direction because the longitudinal gradient force can overcome the longitudinal scattering force at these three points. Figs. 3(b1-b3) present the corresponding transverse gradient forces at these three points. Clearly, the transverse gradient forces go down along the propagation direction after  $z_a=2.983\text{mm}$ . Noted that, the transverse scattering force is so small that it can be neglected. Whatever, according to the simulation, the CSBs do have the ability to capture the Rayleigh particle(20nm). We need to judge whether the particle-trapping of CSBs is stable.

## 6. Analysis of trapping stability

For realizing stable trapping, first of all, the longitudinal gradient force should be large enough to overcome the longitudinal scattering force, as shown in Fig. 3(a1) where the equilibrium points  $z_a, z_b, z_c$  are found. Then, the maximum of longitudinal radiation force should be larger than the difference between buoyancy and gravity ( $10^{-7}$ pN)[21]. In Fig. 3(a2), it is obviously that the largest longitudinal radiation force is larger than  $10^{-7}$ pN.

The third condition is that the potential energy of gradient force should overcome the kinetic of Brownian particle. It can be expressed as follows[21, 33]:

$$\xi = \exp(-U / k_B T) \ll 1 \quad (10)$$

$$U = \frac{1}{4} \varepsilon_0 \varepsilon_m \operatorname{Re}(\alpha) \Delta \left| \bar{\Phi}^2 \right| \quad (11)$$

$$k_B T = 4.14 \times 10^{-21} J, T = 300 K \quad (12)$$

where  $U$  is the potential energy of the gradient force,  $k_B$  is the Boltzmann constant,  $T$  is the thermodynamic temperature of medium, it is assumed that the  $T=300K$ . When incident power is 1W,  $\xi_a = \xi_b = \xi_c = 0$ .

When incident power is 100mW,  $\xi_a = 0.05$ ,  $\xi_b = 0.76$ ,  $\xi_c = 0.64$ . When incident power is 10mW,  $\xi_a = \xi_b = \xi_c = 0.99$ . Obviously, to trap particle stably, the incident power of CSBs cannot be too small. It should be larger than 10mW when adopting the parameters in Fig.3 to generate CSBs.

## 7. Tuning the trapping-force

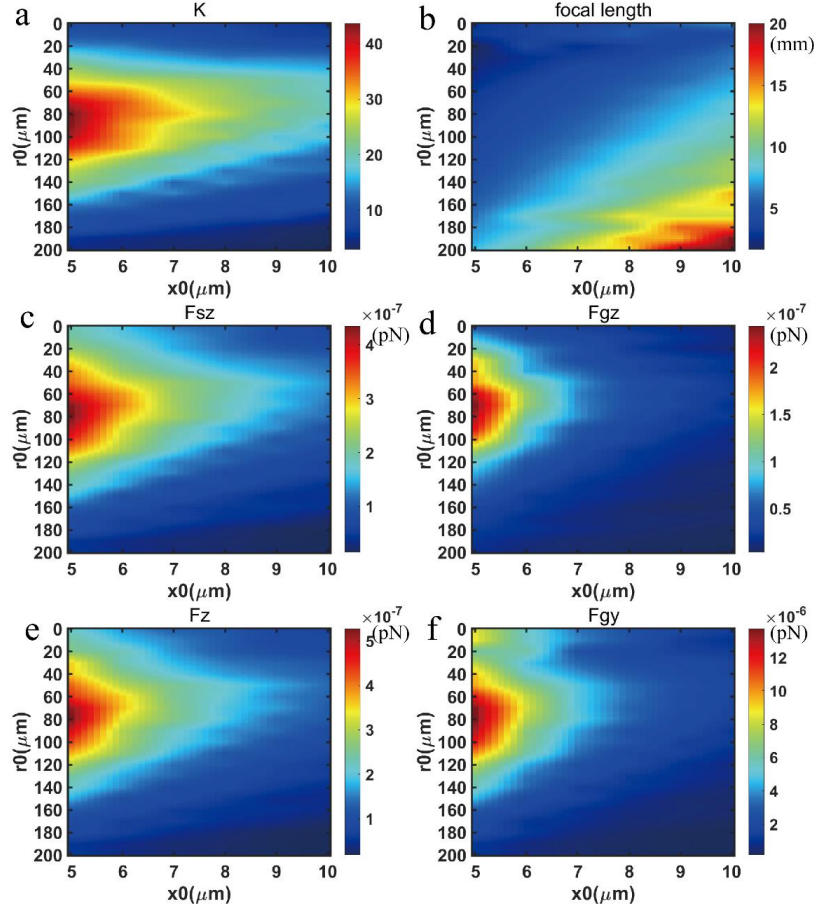


Fig. 4 Trapping force performance of CSBs with changing parameters  $r_0$  and  $x_0$ .  $R_B$  is set to be 0.2mm, the incident power is 1 W. (a) The autofocusing property. (b) the focal length. (c) the longitudinal scattering force. (d) the longitudinal gradient force. (e) the sum of gradient force and scattering force. (f) the transverse gradient force.

By changing the parameters of CSBs, we also analyze the variation of trapping-force at the first focus point with parameters [Fig. 4]. Different from the former control for producing a largest intensity contrast, i.e.,  $r_0 \approx 0.5R_B$  [Fig. 2], the best autofocusing and largest trapping force requires  $r_0 \approx 0.4R_B$  [Figs. 4(a) and (c-f)]. However, the trapping force still increases with a smaller  $x_0$  when the focal length decreases with smaller  $r_0$  and  $x_0$  [Fig. 4(b)]. Noted that, the change of trapping force with  $x_0$  is larger than the case of intensity contrast. In other words, trapping force is more sensitive to the control of the parameters. Moreover, the gradient force goes up faster than scattering force as  $x_0$  increases [Figs. 4(c, d)], indicating a most affected tunability.

## 8. Conclusion

In summary, we have systemically investigated the tunable autofocusing propagation and trapping performance of the CSBs by controlling their beams parameters. Our results show that, the intensity contrast, focal length and largest trapping force decrease with a smaller scale factor  $x_0$  and exhibit maximum as setting an appropriate initial radius of the main ring  $x_0$ . Generally, similar to CABs, CSBs can trap particles stably. Our work is beneficial for the development of optical trapping of CSBs and provide new photonic tools for optical tweezer and manipulation.

### Declaration of Competing Interest

The authors declare that they have no known competing financial interests or personal relationships that could have appeared to influence the work reported in this paper.

### References

1. J. Chen, C. H. Wan, and Q. W. Zhan, "Engineering photonic angular momentum with structured light: a review," *Advanced Photonics* **3**(2021).
2. Y. J. Yang, Y. X. Ren, M. Z. Chen, Y. Arita, and C. Rosales-Guzman, "Optical trapping with structured light: a review," *Advanced Photonics* **3**(2021).
3. "Observation of a single-beam gradient force optical trap for dielectric particles," (1986).
4. C. A. Campugan, K. R. Dunning, and K. Dholakia, "Optical manipulation: a step change for biomedical science," *Contemporary Physics* **61**, 277-294 (2020).
5. P. Polimeno, A. Magazzu, M. A. Iati, R. Saija, L. Folco, D. B. Ciriza, M. G. Donato, A. Foti, P. G. Gucciardi, A. Saidi, C. Cecchi-Pestellini, A. J. Escobar, E. Ammannito, G. Sindoni, I. Bertini, V. D. Corte, L. Inno, A. Ciaravella, A. Rotundi, and O. M. Marago, "Optical tweezers in a dusty universe," *European Physical Journal Plus* **136**(2021).
6. G. A. Siviloglou and D. N. Christodoulides, "Accelerating finite energy Airy beams," *Optics Letters* **32**, 979-981 (2007).
7. H. Cheng, W. P. Zang, W. Y. Zhou, and J. G. Tian, "Analysis of optical trapping and propulsion of Rayleigh particles using Airy beam," *Optics Express* **18**, 20384-20394 (2010).
8. Z. Zheng, B. F. Zhang, H. Chen, J. P. Ding, and H. T. Wang, "Optical trapping with focused Airy beams," *Applied Optics* **50**, 43-49 (2011).
9. I. Kaminer, M. Segev, and D. N. Christodoulides, "Self-Accelerating Self-Trapped Optical Beams," *Physical Review Letters* **106**(2011).
10. J. Broky, G. A. Siviloglou, A. Dogariu, and D. N. Christodoulides, "Self-healing properties of optical Airy beams," *Optics Express* **16**, 12880-12891 (2008).
11. P. Zhang, J. Prakash, Z. Zhang, M. S. Mills, N. K. Efremidis, D. N. Christodoulides, and Z. G. Chen, "Trapping and guiding microparticles with morphing autofocusing Airy beams," *Optics Letters* **36**, 2883-2885 (2011).
12. Y. F. Jiang, K. K. Huang, and X. H. Lu, "Propagation dynamics of abruptly autofocusing Airy beams with optical vortices," *Optics Express* **20**, 18579-18584 (2012).
13. J. D. Ring, J. Lindberg, A. Mourka, M. Mazilu, K. Dholakia, and M. R. Dennis, "Auto-focusing and self-healing of Pearcey beams," *Optics Express* **20**, 18955-18966 (2012).
14. X. Y. Chen, D. M. Deng, J. L. Zhuang, X. Peng, D. D. Li, L. P. Zhang, F. Zhao, X. B. Yang, H. Z. Liu, and G. H. Wang, "Focusing properties of circle Pearcey beams," *Optics Letters* **43**, 3626-3629 (2018).
15. "Dynamics of the optical swallowtail catastrophe," (2017).

16. M. A. Bandres and J. C. Gutierrez-Vega, "Airy-Gauss beams and their transformation by paraxial optical systems," *Optics Express* **15**, 16719-16728 (2007).
17. G. A. Siviloglou, J. Broky, A. Dogariu, and D. N. Christodoulides, "Observation of accelerating airy beams," *Physical Review Letters* **99**(2007).
18. H. I. Sztul and R. R. Alfano, "The Poynting vector and angular momentum of Airy beams," *Optics Express* **16**, 9411-9416 (2008).
19. E. Granot and B. Malomed, "Acceleration of trapped particles and beams," *Journal of Physics B-Atomic Molecular and Optical Physics* **44**(2011).
20. N. K. Efremidis, Z. G. Chen, M. Segev, and D. N. Christodoulides, "Airy beams and accelerating waves: an overview of recent advances," *Optica* **6**, 686-701 (2019).
21. Y. F. Jiang, K. K. Huang, and X. H. Lu, "Radiation force of abruptly autofocusing Airy beams on a Rayleigh particle," *Optics Express* **21**, 24413-24421 (2013).
22. K. Cheng, G. Lu, and X. Q. Zhong, "The Poynting vector and angular momentum density of Swallowtail-Gauss beams," *Optics Communications* **396**, 58-65 (2017).
23. A. Zannotti, F. Diebel, M. Boguslawski, and C. Denz, "Optical catastrophes of the swallowtail and butterfly beams," *New Journal of Physics* **19**(2017).
24. A. Zannotti, F. Diebel, and C. Denz, "Dynamics of the optical swallowtail catastrophe," *Optica* **4**, 1157-1162 (2017).
25. H. A. Teng, Y. X. Qian, Y. P. Lan, and Y. M. Cai, "Abruptly autofocusing circular swallowtail beams," *Optics Letters* **46**, 270-273 (2021).
26. H. A. Teng, Y. X. Qian, Y. P. Lan, and W. T. Cui, "Swallowtail-type diffraction catastrophe beams," *Optics Express* **29**, 3786-3794 (2021).
27. J. J. Jiang, D. L. Xu, Z. W. Mo, X. Z. Cai, H. Y. Huang, Y. Zhang, H. B. Yang, H. Q. Huang, Y. Wu, L. L. Shui, and D. M. Deng, "Generation and control of tornado waves by means of ring swallowtail vortex beams," *Optics Express* **30**, 11331-11344 (2022).
28. Y. Wu, Z. J. Lin, C. J. Xu, D. L. Xu, H. Q. Huang, J. J. Zhao, Z. W. Mo, J. J. Jiang, H. B. Yang, L. P. Zhang, H. Z. Liu, D. M. Deng, and L. L. Shui, "Abruptly Autofocusing Twisted Optical Bottle Beams," *Physical Review Applied* **17**(2022).
29. Y. Zhang, J. L. Tu, S. L. He, Y. P. Ding, Z. L. Lu, Y. Wu, G. H. Wang, X. B. Yang, and D. M. Deng, "Experimental generation of the polycyclic tornado circular swallowtail beam with self-healing and auto-focusing," *Optics Express* **30**, 1829-1840 (2022).
30. F. Lu, H. Wu, Y. Liang, L. Tan, Z. Tan, X. Feng, Y. Hu, Y. Xiang, X. Hu, Z. Chen, and J. Xu, "Bessel-modulated autofocusing beams for optimal trapping implementation," *Physical Review A* **104**(2021).
31. F. Lu, L. Tan, Z. Tan, H. Wu, and Y. Liang, "Dynamical power flow and trapping-force properties of two-dimensional Airy-beam superpositions," *Physical Review A* **104**(2021).
32. Y. F. Jiang, K. K. Huang, and X. H. Lu, "Radiation force of highly focused Lorentz-Gauss beams on a Rayleigh particle," *Optics Express* **19**, 9708-9713 (2011).
33. Z. Liu, X. Wang, and K. Hang, "Enhancement of trapping efficiency by utilizing a hollow sinh-Gaussian beam," *Scientific Reports* **9**(2019).